ACS APPLIED MATERIALS & INTERFACES

Letter

www.acsami.org

Synthesis of near-Infrared Quantum Dots in Cultured Cancer Cells

Lianjiang Tan,[†] Ajun Wan,*[,†] and Huili Li[‡]

[†]School of Chemistry and Chemical Engineeringand [‡]School of Pharmacy, Shanghai Jiao Tong University, Shanghai, 200240, China

Supporting Information

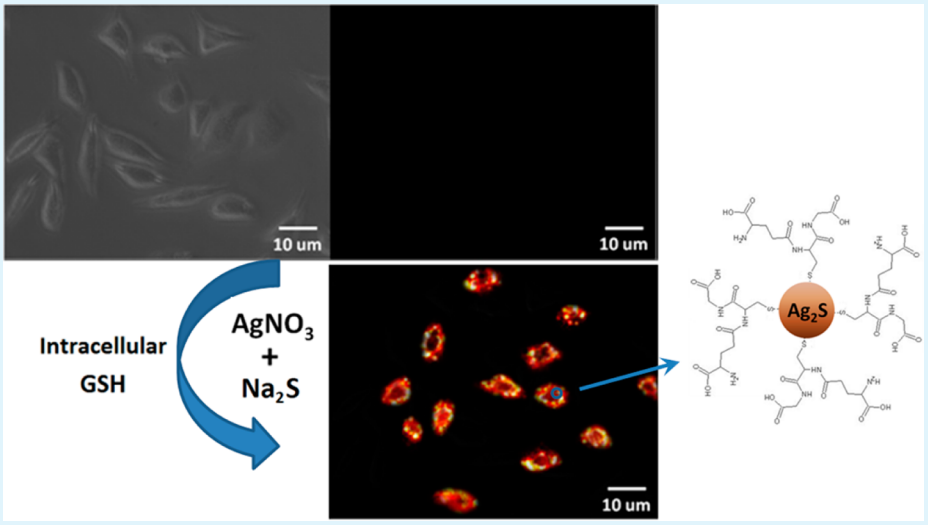

ABSTRACT: Intracellular synthesis of near-infrared fluorescent silver sulfide quantum dots in HepG2 cancer cells is demonstrated. By delivering quantum dot precursors into cultured hepatoma carcinoma cells (HepG2 cells), silver sulfide quantum dots with emission efficiency qualified for in vivo imaging were successfully synthesized with the aid of endogenous glutathione in the cells.

KEYWORDS: *Ag_2S quantum dots, near-infrared emission, synthesis, cancer cells*

1. INTRODUCTION

In recent years, quantum dots (QDs) have attracted great attention as biological labeling and imaging agents due to their distinguished characteristics such as robust fluorescence intensity, broad excitation wavelength range, narrow and symmetrical emission spectra, great photostablility, etc.[1−4] Fluorescence in the near-infrared (NIR) region penetrates deep in the body, with less scattering and absorption and reduced autofluorescence of tissue and blood, which make it advantageous for live animal imaging.[5−8] However, the lack of biocompatible fluorescent probes in the NIR region limited the utilization of this highly sensitive spectral range for bioimaging.[9−11] Nanoscaled silver chalcogenides, which have low toxicity and narrow band gaps, have been reported as promising candidates for NIR fluorescent quantum dots.[12−15] Silver sulfide (Ag_2S) nanocrystals with excellent optical properties and negligible toxicity have been synthesized.[16,17] Moreover, the use of biological molecules for the synthesis of Ag_2S quantum dots results in biomolecule-conjugated NIR fluorescent nanomaterials with bioactive surface and targeting function.[18,19]

Biosynthesis of semiconductor nanocrystals was first reported in unicellular yeast, which was demonstrated to be able to produce cadmium sulphide (CdS) quantum dots subject to challenge by a cadmium salt.[20] Cd-containing quantum dots have been synthesized using fungi, bacteria, or yeast.[21−26] Glutathione often played a pivotal role in the intracellular biosynthesis of the quantum dots, either as a reducing agent or sulfur source or both. The optical properties of the biosynthesized quantum dots are similar to those of their chemically synthesized counterparts. Also, intrinsically toxic PbS quantum dots emitting in NIR region was synthesized in microorganisms.[27] More recently, synthesis of CdTe quantum dots has been successfully conducted in earthworms.[28] These interesting findings have inspired us to explore other biosynthetic routes for fabricating photoluminescent nanocrystals. It is well-known that reduced glutathione (GSH) is an abundant natural tripeptide found within almost all cells. In cancer cells, the concentration of GSH (2−8 mM) is usually much higher than that in normal cells.[29−31] The unique intracellular high GSH content provides an inbuilt advantage for the synthesis of fluorescent quantum dots in cancer cells, as

Received: October 15, 2013
Accepted: December 17, 2013
Published: December 17, 2013

Scheme 1. Synthetic Strategy of Ag_2S Quantum Dots in Cultured HepG2 Cancer Cells

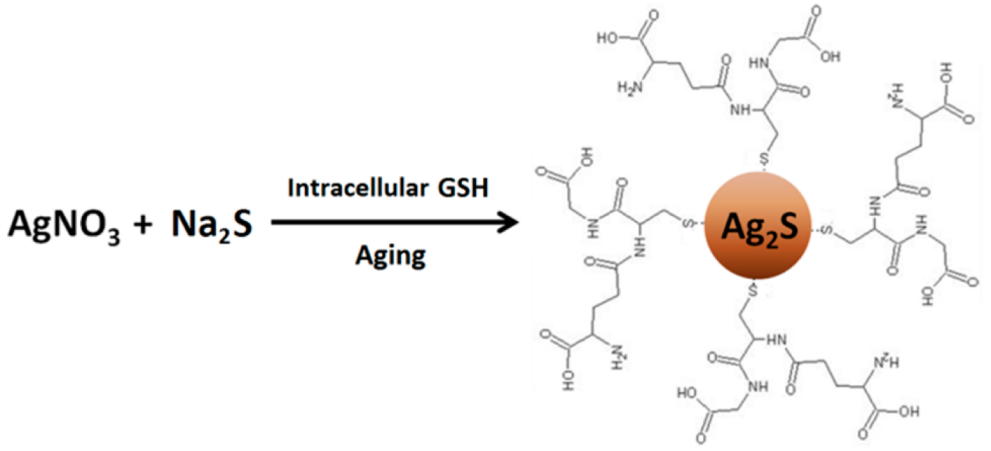

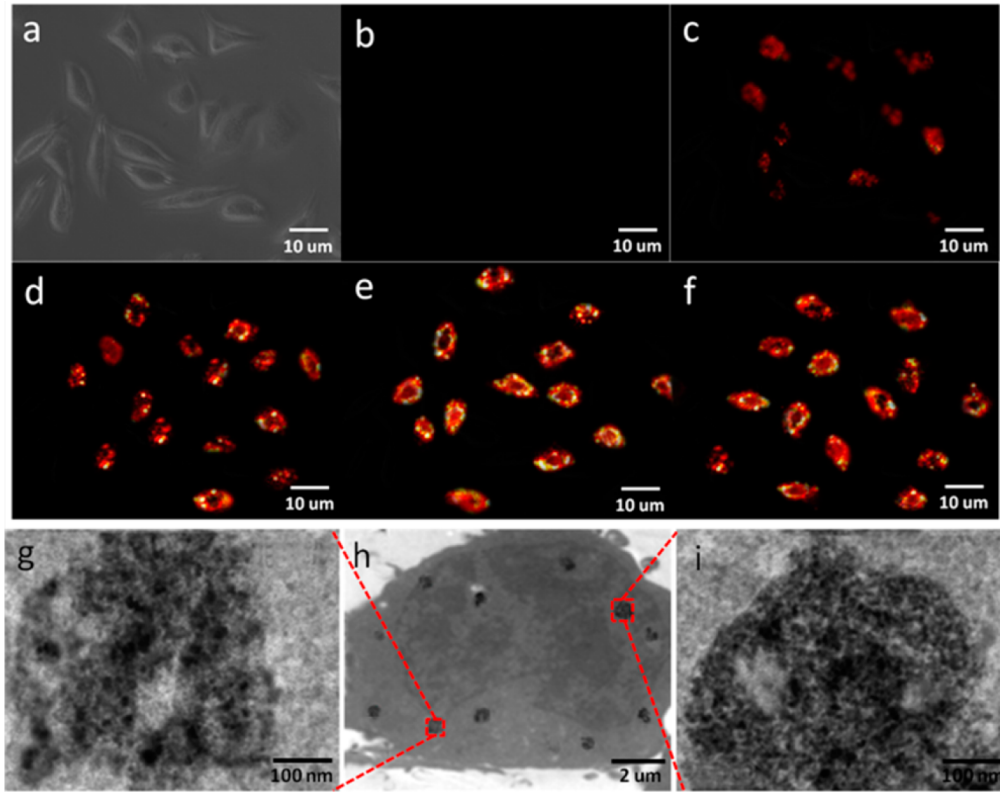

Figure 1. (a) Bright-field image and (b) NIR image of HepG2 cells immediately after uptake of silver nitrate and sodium sulfide. NIR images of HepG2 cells at (c) 8, (d) 12, (e) 16, and (f) 20 h after uptake of silver nitrate and sodium sulfide. (h) TEM image of a HepG2 cancer cell containing synthesized Ag_2S quantum dots; (g, i) TEM images of the Ag_2S quantum dots denoted by the red dashed boxes in h.

the GSH is an excellent surface stabilizer for the formation of quantum dots.[32,33] Herein, we present unprecedented intracellular synthesis of GSH-stabilized Ag_2S quantum dots in cultured cancer cells (Scheme 1). The quantum dot precursors, silver nitrate and sodium sulfide, were internalized by cultured hepatoma carcinoma cells (HepG2 cells) successively. The cell temperature is able to drive the reaction between the precursors, though the synthetic process needs prolonged time compared with those under regular chemical synthesis conditions. The endogenous GSH in the cells coordinates with the nanoparticles during the reaction and prevents them from coalescing to form bulk Ag_2S crystals. The synthesized Ag_2S quantum dots were obtained by isolating them from the cells. We chose to work with HepG2 cells, a type of liver cancer cells because they contain a high concentration of GSH that can strongly favor the intracellular formation of Ag_2S quantum dots.

2. RESULTS AND DISCUSSION

The cultured HepG2 cells containing quantum dot precursors (Figure 1a) were monitored using an NIR-sensitive InGaAs camera. The received NIR signals were processed and coded, and expressed by pseudocolor in an image. There was no detectable emission signal from the cells at the beginning of the aging process (Figure 1b). After 20 h, NIR fluorescence emission was observed (Figure 1c), the signal of which increased with prolonged aging time of 16 h (Figure 1d, e).

dx.doi.org/10.1021/am404534v | ACS Appl. Mater. Interfaces 2014, 6, 18−23

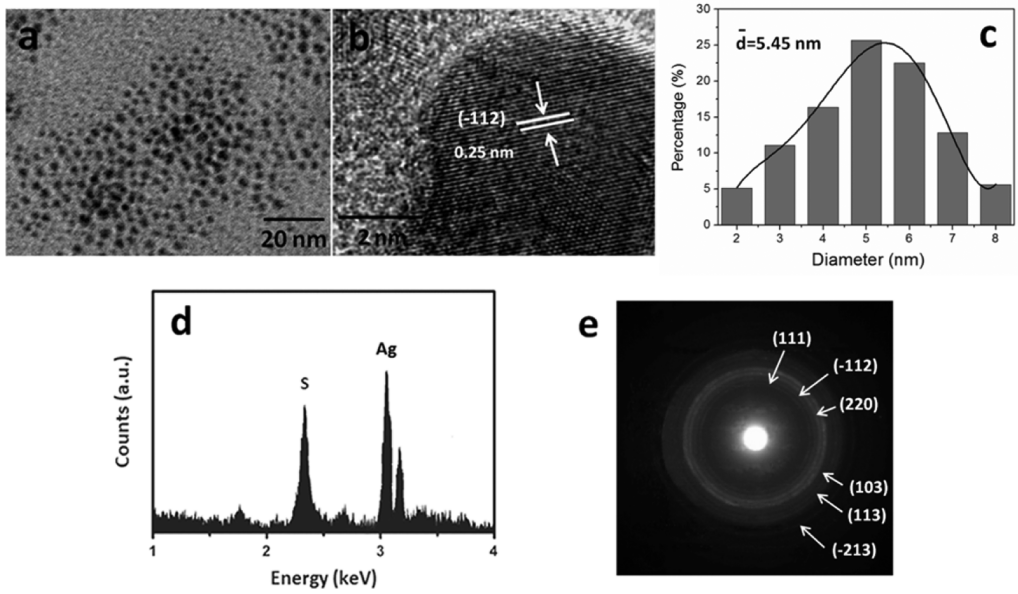

Figure 2. (a, b) High-resolution TEM images and (c) corresponding size distribution histograms of as-isolated Ag_2S quantum dots. (d) EDX spectrum of the Ag_2S quantum dots. (e) SAED pattern of the Ag_2S quantum dots and the assinged Miller indices.

In control experiments, blank HepG2 cells, and HepG2 cells treated only with silver nitrate or sodium sulfide were imaged and they all showed no observable NIR signals (Figure S1, see the Supporting Information). The emission signal was a little weaker at 20 h than that at 16 h (Figure 1f). The intensity of total photons emitted from the cells was plotted as a function of time (see Figure S2 in the Supporting Information). The fluorescence intensity increased with time to a maximum at 16 h, and then leveled off. The quantum dots retained over 85% of the maximum fluorescence intensity at 24 h postadministration of the quantum dot precursors. TEM micrographs of a HepG2 cell show nanoparticle clusters in cytoplasm of the cells (Figure 1g–i), revealing the intracellular formation of Ag_2S quantum dots at 16 h postadministration of the quantum dot precursors. The existence of Ag_2S quantum dots in the cytoplasm was further confirmed by EDX analysis of the precursors-containing cells incubated for 16 h (see Figure S3 in the Supporting Information). The quantum dot precursors reacted in the cells over a period, during which an increasing number of quantum dots formed. Measured via the enzymatic cycling method, the GSH concentration in the cultured HepG2 cells was 30.9 ± 4.6 mg/g pro, whereas the GSH concentration in cultured L929 cells (mouse fibroblast cells) was only 7.7 ± 2.2 mg/g pro, indicating high GSH content in the HepG2 cells compared with normal cells. We also measured the GSH concentration in the precursors-containing HepG2 cells during the aging process, giving 19.1 ± 4.0, 16.8 ± 3.8, 15.1 ± 4.1, and 14.5 ± 3.6 mg/g pro at 8, 12, 16, and 20 h, respectively. In contrast, the GSH concentration in blank HepG2 cells was 31.2 ± 5.6, 30.2 ± 5.2, 29.9 ± 4.6 and 29.0 ± 3.9 mg/g pro at the corresponding time point. It is evident that GSH was consumed during the synthesis of Ag_2S quantum dots. The intracellular GSH keeps the nanocrystals from coalescing and facilitates the formation of quantum dots with narrow size distribution, because the GSH is an effective stabilizer by terminating the quantum dots with carboxylic acid groups. Fourier transform infrared (FTIR) spectrum of the as-synthesized Ag_2S quantum dots isolated from the cells (see Figure S4 in the Supporting Information) was recorded. The absorption peak at 2568 cm^{-1} is typical of free thiol group. The peak at 1708 cm^{-1} is ascribed to the C═O stretch vibration of carboxyl group, and the one at 1660 cm^{-1} corresponds to the C═O stretching of amide (amide I). The FTIR spectrum is characteristic of GSH, demonstrating that the endogenous GSH coordinates with the biosynthesized Ag_2S quantum dots. It is noted that the Ag_2S quantum dots formed over 12 h' aging of the cells, as reflected by the readily observable NIR emission. Continued aging for another 4 h led to even stronger emission, suggesting that the synthesis of quantum dots proceeded up to extended time of 16 h. The intracellular synthetic yield grew with time and hence the fluorescence emission from the cells increased during the 16 h. The emission intensity no longer increased as the cells were further aged, indicating that 16 h is sufficient for the synthesis of Ag_2S quantum dots in the cultured HepG2 cells. The cytotoxicity of the quantum dot precursors during the aging process in the cells was evaluated by both MTT and trypan blue assays (see Figure S5 in the Supporting Information). At 12 h postadministration, more than 85% of the cells survived relative to the control, suggesting that intracellular synthesis of Ag_2S quantum dots could be safely carried out. After 12 h, the Ag_2S quantum dots formed, and the cell viability changed slightly with time up to 24 h, as the Ag_2S quantum dots are extremely low toxic.

The morphology of as-synthesized Ag_2S quantum dots was observed by transmission electron microscopy (TEM) (Figure 2a, b). The high-resolution TEM micrograph (Figure 2b) clearly indicates lattice fringes of the nanocrystals with an interplanar spacing of ~0.25 nm, assigned to the (−1, 1, 2) facets of a monoclinic α-Ag_2S crystal. The size distribution histogram obtained by measuring the diameter of 200 nanoparticles in a TEM image shows an average size of 5.45 nm (Figure 2c). Energy dispersive X-ray (EDX) analysis (Figure 2d) gave an atomic ratio (Ag/S = 56.9/43.1) comparable to the stoichiometry of bulk Ag_2S, indicating the presence of elements Ag and S in the samples. The higher sulfur content is most likely due to the GSH coordinated to the nanoparticle surface. The X-ray photoelectron spectroscopy (XPS) results (see Figure S6 in the Supporting Information)

dx.doi.org/10.1021/am404534v | ACS Appl. Mater. Interfaces 2014, 6, 18−23

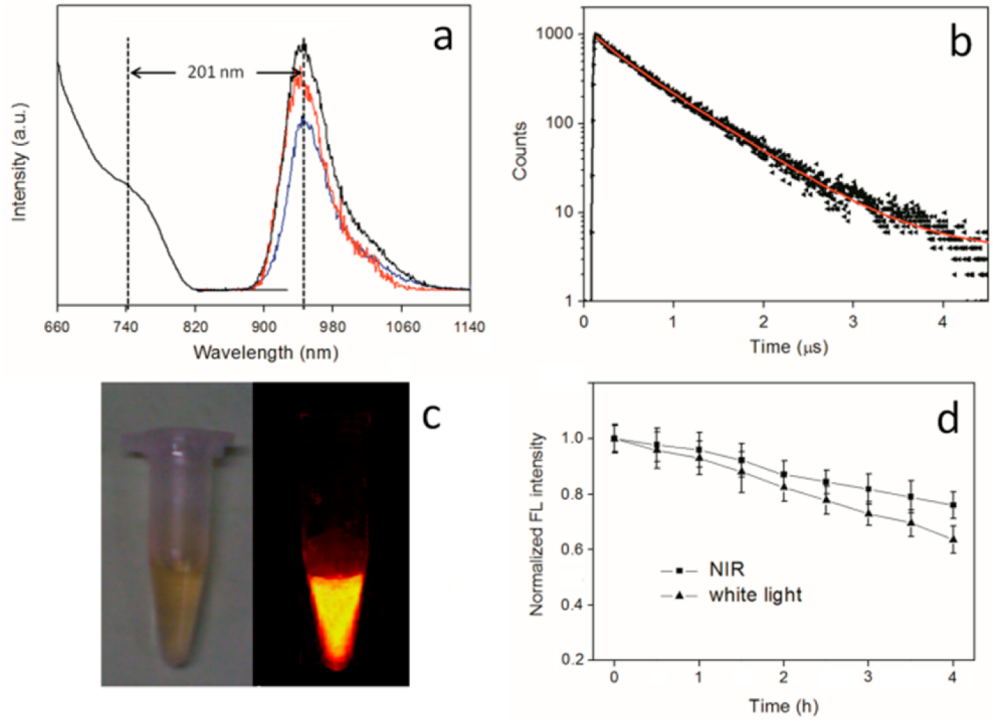

Figure 3. (a) Absorption of as-isolated Ag_2S quantum dots at 16 h postadministration of quantum dot precursors in the HepG2 cells (left). NIR emission spectra of as-isolated Ag_2S quantum dots at varied times postadministration of quantum dot precursors in the cells (right): 16, 20, and 12 h, from top to bottom. (b) Fluorescence lifetime measurements of emission from as-isolated Ag_2S quantum dots, exhibiting two emissive species: biexponential fitting corresponding to τ_1 = 204.7 ± 8.52 ns, τ_2 = 655.6 ± 15.1 ns. (c) Bright-field and NIR fluorescence images of the Ag_2S quantum dots aqueous solution. (d) Photostability of the Ag_2S quantum dots under irradiation of 758 nm laser and white light at the power of 100 W.

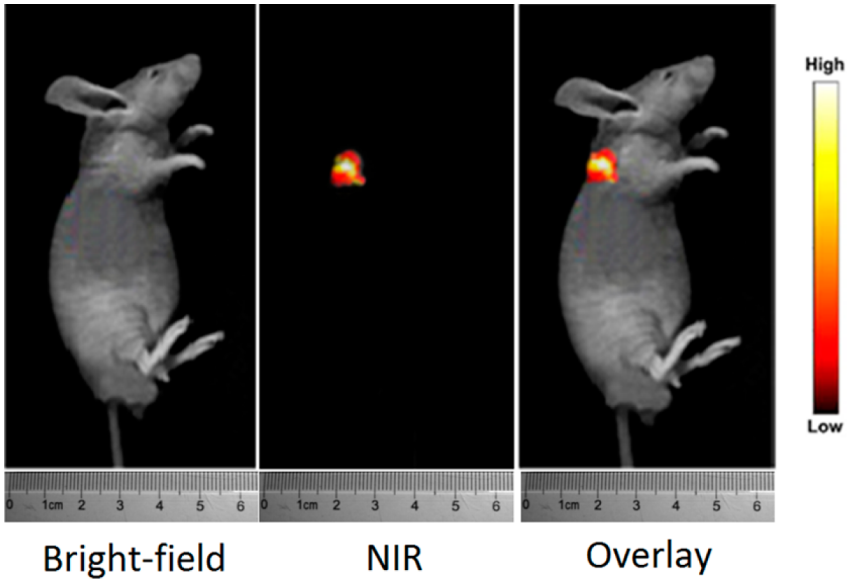

Figure 4. Bright-field image, in vivo NIR fluorescence image, and the merged image of a nude mouse at 5 min after subcutaneous injection of the intracellularly synthesized Ag_2S quantum dots. The autofluorescence of the mice in the NIR region was fairly weak and was subtracted by the imaging system.

indicate that the oxidation state of Ag ion was univalent in the Ag_2S quantum dots. Selected area electron diffraction (SAED) image (Figure 2e) displayed diffraction rings characteristic of Ag_2S nanocrystals. The X-ray diffraction (XRD) results confirmed the monoclinic nature of the Ag_2S quantum dots (see Figure S7 in the Supporting Information).

The synthesized Ag_2S quantum dots at 16 h postadministration of the quantum dot precursors showed an absorption at 744 nm with a band edge at ~820 nm (Figure 3a). The emission peak was situated at 945 nm, the full width at half-maximum (fwhm) of which was 66 nm. A large Stokes shift (201 nm) means less disturbance of excitation light to the fluorescence emission of the quantum dots. The emission quantum yield (QY) was calculated to be 1.56 ± 0.21% against indocyanine green in DMSO (QY = 13%), similar to those of chemically synthesized Ag_2S quantum dots.[18,34] We also

dx.doi.org/10.1021/am404534v | ACS Appl. Mater. Interfaces 2014, 6, 18−23

recorded the emission spectra of the nanoparticles isolated from the HepG2 cells at 12 and 20 h postadministration of the precursors (Figure 3 a). The emission peaks of the two samples were located at 943 and 941 nm, respectively, similar to the peak location of the sample at 16 h. The emission intensity of the two samples relative to the sample at 16 h agreed well with the results of the cell fluorescence images in Figure 1. The fluorescence lifetime measurements of the quantum dots (Figure 3 b) showed two decay components, a longer component (655.6 ns) typical of Ag_2S quantum dots[19] and a shorter one (204.7 ns) likely ascribed to nonradiative recombination centers at the quantum dot surface or exciton scattering. The NIR emission from the aqueous solution of the quantum dots was observed by the NIR-sensitive camera (Figure 3c). The photostability of the quantum dots was examined (Figure 3d): 75.9 and 63.6% of the original fluorescence intensity were retained after 4 h of continuous irradiation of 758 nm NIR laser and white light, respectively, indicative of excellent photostability of the quantum dots.

To demonstrate the in vivo imaging ability of the intracellularly synthesized Ag_2S quantum dots, small animal imaging experiment was performed. Ag_2S quantum dots were administered into a group of anesthetized nude mice by subcutaneous injection, respectively. The mice were then imaged under 758 nm laser excitation. As indicated in Figure 4, the NIR fluorescence signals derived from the Ag_2S quantum dots were clearly observed in the injection region of the mice at 5 min postadministration. The readily detectable signals indicated the strong tissue penetrability of the NIR fluorescence emitted by the Ag_2S quantum dots. The high contrast of the images resulted from the deep tissue penetration of NIR fluorescence suggests the excellent imaging ability of the Ag_2S quantum dots.

3. CONCLUSION

In conclusion, we have synthesized the NIR fluorescent Ag_2S quantum dots in cultured HepG2 cancer cells. Quantum dot precursors were delivered into the cells, where they reacted to produce quantum dots under the action of endogenous GSH. The high GSH content in the cancer cells favored the intracellular synthesis of the quantum dots. The resultant Ag_2S quantum dots exhibited high emission efficiency and good optical stability, with a quantum yield eligible for in vitro and in vivo imaging. In consideration of the possible extension to intracellular synthesis of various fluorescent quantum dots using proper precursors, the addressed synthetic strategy offers new insights for preparing bioimaging agents.

■ ASSOCIATED CONTENT

Ⓢ Supporting Information

Relevant experimental results and data not included in the manuscript. This material is available free of charge via the Internet at http://pubs.acs.org/.

■ AUTHOR INFORMATION

Corresponding Author

*E-mail: wanajun@sjtu.edu.cn. Fax: 86-21-34201245. Tel: 86-21-34201245.

Notes

The authors declare no competing financial interest.

■ ACKNOWLEDGMENTS

This work was financially supported by the Specialized Research Fund for the Doctoral Program of Higher Education (20130073120087), the Shanghai Postdoctoral Sustentation Fund (13R21413800 and 13R21413900), the China Postdoctoral Science Foundation (2013M531164), the National Natural Science Foundation (51173104 and 21076124), and the Nanometer Technology Program of Science and Technology Committee of Shanghai (11 nm0503500).

■ REFERENCES

(1) Wu, Q.; Chu, M. *Int. J. Nanomed.* **2012**, *7*, 3433−3443.
(2) Fan, J.; Chu, P. K. *Small* **2010**, *6*, 2080−2098.
(3) Smith, A. M.; Mancini, M. C.; Nie, S. *Nat. Nanotechnol.* **2009**, *4*, 710−711.
(4) Medintz, I. L.; Uyeda, H. T.; Goldman, E. R.; Mattoussi, H. *Nat. Mater.* **2005**, *4*, 435−446.
(5) Robinson, J. T.; Hong, G. S.; Liang, Y. Y.; Zhang, B.; Yaghi, O. K.; Dai, H. J. *J. Am. Chem. Soc.* **2012**, *134*, 10664−10669.
(6) Welsher, K.; Sherlock, S. P.; Dai, H. *Proc. Nat. Acad. Sci.U.S.A.* **2011**, *108*, 8943−8948.
(7) Welsher, K.; Liu, Z.; Sherlock, S. P.; Robinson, J. T.; Chen, Z.; Daranciang, D.; Dai, H. *Nat. Nanotechnol.* **2009**, *4*, 773−780.
(8) Weissleder, R. *Nat. Biotechnol.* **2001**, *19*, 316−317.
(9) Du, H.; Chen, C. L.; Krishnan, R.; Krauss, T. D.; Harbold, J. M.; Wise, F. W.; Thomas, M. G.; Silcox, J. *Nano Lett.* **2002**, *2*, 1321−1324.
(10) Moreels, I.; Justo, Y.; De Geyter, B.; Haustraete, K.; Martins, J. C.; Hens, Z. *ACS Nano* **2011**, *5*, 2004−2012.
(11) Xie, R.; Battaglia, D.; Peng, X. *J. Am. Chem. Soc.* **2007**, *129*, 15432−15433.
(12) Ma, X. H.; Zhao, Y. Y.; Jiang, X. Y.; Liu, W.; Liu, S. Q.; Tang, Z. Y. *ChemPhysChem* **2012**, *13*, 2531−2535.
(13) Khanna, P. K.; Das, B. K. *Mater. Lett.* **2004**, *58*, 1030−1034.
(14) Zhu, C. N.; Jiang, P.; Zhang, Z. L.; Zhu, D. L.; Tian, Z. Q.; Pang, D. W. *ACS Appl. Mater. Interfaces.* **2013**, *5*, 1186−1189.
(15) Gu, Y. P.; Cui, R.; Zhang, Z. L.; Xie, Z. X.; Pang, D. W. *J. Am. Chem. Soc.* **2012**, *134*, 79.
(16) Wang, C.; Wang, Y.; Xu, L.; Zhang, D.; Liu, M.; Li, X.; Sun, H.; Lin, Q.; Yang, B. *Small* **2012**, *8*, 3137−3142.
(17) Hocaoglu, I.; Cizmeciyan, M. N.; Erdem, R.; Ozen, C.; Kurt, A.; Sennaroglu, A.; Acar, H. Y. *J. Mater. Chem.* **2012**, *22*, 14674.
(18) Yang, H. Y.; Zhao, Y. W.; Zhang, Z. Y.; Xiong, H. M.; Yu, S. N. *Nanotechnology* **2013**, *24*, 055706.
(19) Wang, Y.; Yan, X. P. *Chem. Commun.* **2013**, *49*, 3324−3326.
(20) Dameron, C. T.; Reese, R. N.; Mehra, R. K.; Kortan, A. R.; Carroll, P. J.; Steigerwald, M. L.; Brus, L. E.; Winge, D. R. *Nature* **1989**, *338*, 596−597.
(21) Kumar, S. A.; Ansary, A. A.; Ahmad, A.; Khan, M. I. *J. Biomed. Nanotechnol.* **2007**, *3*, 190−194.
(22) Pérez-Donoso, J. M.; Monrás, J. P.; Bravo, D.; Aguirre, A.; Quest, A. F.; Osorio-Román, I. O.; Aroca, R. F.; Chasteen, T. G.; Vásquez, C. C. *PLoS ONE* **2012**, *7*, e30741.
(23) Monrás, J. P.; Diaz, V.; Bravo, D.; Montes, R. A.; Chasteen, T. G.; Osorio-Román, I. O.; Vásquez, C. C.; Pérez-Donoso, J. M. *PLoS ONE* **2012**, *7*, e48657.
(24) Cui, R.; Liu, H.; Xie, H.; Zhang, Z.; Yang, Y.; Pang, D.; Xie, Z.; Chen, B.; Hu, B.; Shen, P. *Adv. Funct. Mater.* **2009**, *19*, 2359−2364.
(25) Sweeney, R. Y.; Mao, C.; Gao, X.; Burt, J. L.; Belcher, A. M.; Georgiou, G.; Iverson, B. L. *Chem. Biol.* **2004**, *11*, 1553−1559.
(26) Li, Y.; Cui, R.; Zhang, P.; Chen, B. B.; Tian, Z. Q.; Li, L.; Hu, B.; Pang, D. W.; Xie, Z. X. *ACS Nano* **2013**, *7*, 2240−2248.
(27) Kowshik, M.; Vogel, W.; Urban, J.; Kulkarni, S. K.; Paknikar, K. M. *Adv. Mater.* **2002**, *14*, 815−818.
(28) Sturzenbaum, S. R.; Höckner, M.; Panneerselvam, A.; Levitt, J.; Bouillard, J. S.; Taniguchi, S.; Dailey, L. A.; Ahmad, K. R.; Rosca, E. V.; Thanou, M.; Suhling, K.; Zayats, A. V.; Green, M. *Nat. Nanotechnol.* **2013**, *8*, 57−60.

(29) Zheng, Z. B.; Zhu, G. Z.; Tak, H.; Joseph, E.; Eiseman, J. L.; Creighton, D. J. *Bioconjugate. Chem* **2005**, *16*, 598−607.
(30) Balendiran, G. K.; Dabur, R.; Fraser, D. *Cell. Biochem. Funct.* **2004**, *22*, 343−352.
(31) Schafer, F. Q.; Buettner, G. R. *Free Radical Biol. Med.* **2001**, *30*, 1191−1212.
(32) Jin, T.; Fujii, F.; Komai, Y.; Seki, J.; Seiyama, A.; Yoshioka, Y. *Int. J. Mol. Sci.* **2008**, *9*, 2044−2061.
(33) Yuana, J.; Guo, W.; Yin, J.; Wang, E. *Talanta* **2009**, *77*, 1858−1863.
(34) Jiang, P.; Zhu, C. N.; Zhang, Z. L.; Tian, Z. Q.; Pang, D. W. *Biomaterials* **2012**, *33*, 5130−5135.